

Rapid control prototyping platform for PV systems based on Arduino and Simulink.



Revista EIA
ISSN 1794-1237
e-ISSN 2463-0950
Año XVIII/ Volumen 18/ Edición N.36
Junio-Diciembre de 2021
Reia36002 pp. 1-21

Publicación científica semestral
Universidad EIA, Envigado, Colombia

DANIEL GONZÁLEZ-MONTOYA¹

✉ JUAN ESTEBAN ZABALA-DAZA¹

ELKIN EDILBERTO HENAO-BRAVO¹

CARLOS ANDRÉS RAMOS-PAJA²

DIEGO ANDRÉS APONTE-ROA³

PARA CITAR ESTE ARTÍCULO / TO REFERENCE THIS ARTICLE /

González-Montoya, D.; Zabala-Daza, J.E.; Henao-Bravo, E.E.; Ramos-Paja, C.A.; Aponte-Roa, D.A. (2021).

Rapid control prototyping platform for PV systems based on Arduino and Simulink.

Revista EIA, 18(36), Reia36002.

pp. 1-21.

<https://doi.org/10.24050/reia.v18i36.1470>

v18i36.1470

✉ *Autor de correspondencia:*

Zabala-Daza, J.E. (Juan Esteban):
Ingeniero Mecatrónico. Instituto
Tecnológico Metropolitano
Correo electrónico:
juanzabala139525@correo.itm.edu.co

Recibido: 20-09-2020

Aceptado: 10-05-2021

Disponible online: 01-06-2021

1. Instituto Tecnológico Metropolitano
2. Universidad Nacional de Colombia
3. Universidad Ana G. Méndez. Gurabo, Puerto Rico

Abstract

This paper presents the development and testing of a Rapid Control Prototyping (RCP) platform for PV systems. The proposed platform is intended to support the evaluation of both PV voltage controllers and MPPT algorithms, devoted to PV systems, without the need of constructing a testbench for each application. Instead, the platform provides a unified experimental environment, easy-to-use, for testing control strategies under realistic conditions, prior to their final implementation in commercial devices. The proposed RCP system is capable of measuring, in real-time, physical variables needed to evaluate the behavior of the control strategies, without constructing dedicated sensors or using costly equipment. The platform is based on the combination of low-cost hardware (Arduino board) and commonly available software (Matlab/Simulink), which provides an easy-to-use environment for non-experts in programming embedded devices. The RCP system usability is validated using a classical PI voltage controller and perturb and observe MPPT algorithm, but any other control strategies can be tested. Finally, the results show that the proposed platform provide similar results in comparison with detailed simulations, which confirms the correct implementation of both the voltage controller and MPPT algorithm by means of the RCP platform.

Key Words: RCP, P&O, MPPT algorithm, Simulink, Arduino.

Plataforma de prototipos de control rápido para sistemas fotovoltaicos basados en Arduino y Simulink.

Resumen

En este documento se presenta el desarrollo y ensayo de una plataforma de prototipos de control rápido (RCP) para sistemas fotovoltaicos. La plataforma propuesta tiene por objeto apoyar la evaluación tanto de los controladores de tensión de los sistemas fotovoltaicos como de los algoritmos MPPT, dedicados a los sistemas fotovoltaicos, sin necesidad de construir un banco de pruebas para cada aplicación. En cambio, la plataforma proporciona un entorno experimental unificado, fácil de utilizar, para probar las estrategias de control en condiciones realistas, antes de su aplicación final en los dispositivos comerciales. El sistema RCP propuesto es capaz de medir, en tiempo real, las variables físicas necesarias para evaluar el comportamiento de las estrategias de control, sin necesidad de construir sensores dedicados o utilizar equipos costosos. La plataforma se basa en la combinación de hardware de bajo costo (placa Arduino) y software comúnmente disponible (Matlab/Simulink), que proporciona un entorno fácil de usar para los no expertos en la programación de dispositivos incorporados. La usabilidad del sistema RCP se valida utilizando un controlador de tensión PI clásico y perturba y observa el algoritmo MPPT, pero se puede probar cualquier otra estrategia de control. Por último, los resultados muestran que la plataforma propuesta proporciona resultados similares en comparación con las simulaciones detalladas, lo que confirma la correcta implementación tanto del controlador de tensión como del algoritmo MPPT mediante la plataforma RCP.

Palabras Claves: RCP, P&O, Algoritmo MPPT, Simulink, Arduino.

Introduction

In the last few years, the interconnection of distributed generation units (DGs), including photovoltaic (PV) generators and wind turbines, among others, has raised due to the growing demand for electricity and the fast depletion of fossil fuels (Petroni & Ramos-Paja, 2011). To combine those distributed sources, power electronics converters play a vital role in wide range of applications such as grid integration of renewable energy systems, battery charger/discharger systems, electric and hybrid electric vehicles, uninterruptible power supplies, among others (Eghtedarpour & Farjah, 2012; Serna-Garcés et al., 2016; Zeng et al., 2013). Rapid Control Prototyping (RCP) provides a good alternative to validate the control strategies in emulated conditions similar to the real ones (Lee et al., 2017). In addition, RCP improves the control design process of the selected application by means of easy-to-use hardware and software interfaces, which reduces the development time by allowing corrections to the control algorithm before the final implementation. The RCP process considers a board with I/O ports to execute the C code generated by an interconnected computer, in which the control algorithms are implemented using block diagrams, i.e. Matlab/Simulink, Lab-View (Grepl, 2011). MATLAB is a software widely adopted to design algorithms and analyze data, and in combination with Simulink, it enables the modeling and simulation of dynamic systems with a comfortable user interface environment. In such a way, MATLAB/Simulink is widely used by researchers in the evaluation of maximum power point tracking (MPPT) techniques for PV applications (de Brito et al., 2013; Eghtedarpour & Farjah, 2012; Salah et al., 2015; Winston et al., 2018). In recent years, MATLAB/

Simulink has been incorporated in the classroom for teaching power electronics and electrical machines courses, this with the aims of reinforcing concepts and to provide a simulation and modeling environment of power systems to enhance the knowledge of future engineers (Boscaino et al., 2013; Restrepo et al., 2012; Smedsgaard, 2006). On the Hardware side, the most popular prototyping platform used by researchers and educators is the Arduino line (Claros-Marfil et al., 2016; Müller et al., 2015; Ulloa et al., 2017). However, such a platform has not been extensively exploited in the teaching of power electronics courses, even though it provides a fast learning process. By combining the advantages that both platforms (Simulink and Arduino), students and researchers will be able to develop control strategies for switched converters without significant hardware implementations and with the possibility of developing algorithms in a friendly environment, and in some cases, on-line.

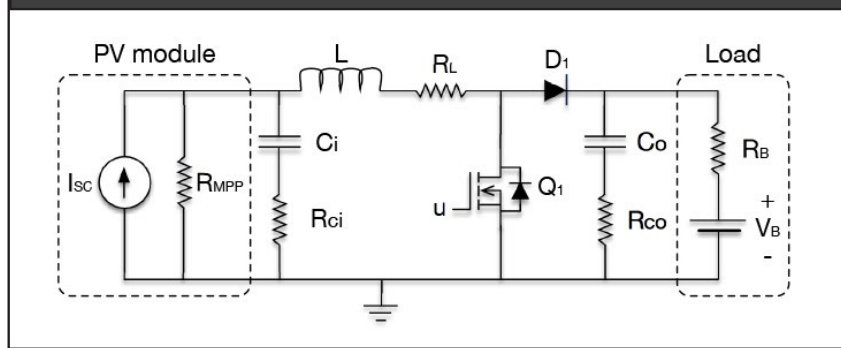
In the renewable energy field, at an educational and commercial level, the extraction of the maximum energy available in the system is a common goal in which power converters are fundamental elements. Hence, the control of the variables of those converters will allow designers to develop and tune MPPT devices to specific conditions (Eghtedarpour & Farjah, 2012; Hossain et al., 2018). Thus, this paper focuses on the development of a RCP platform to test control strategies for power converters used in PV applications, which is based on both Arduino and Simulink tools. The rest of the paper is organized as follows: Section II presents the modelling of the proposed system for control purposes. In addition, such a section describes the methodology of the software and hardware setup used for the RCP implementation. Section III is dedicated to the discussion of the results obtained in the prototype, in comparison with simulated data, to validate the proposed system. Finally, Section IV provides concluding remarks regarding the feasibility of using the proposed platform in real PV applications.

Methodology

Modelling the PV system for control purposes

Figure 1 presents the classical solution used to implement a PV system. Such a power system is controlled using a Pulse Width Modulator (PWM), where the duty cycle D is constantly modified to find the optimum operating point in which the PV module produces the maximum power (MPP) (Trejos et al., 2012). The selected DC/DC converter has a Boost topology due to its extensive use in grid-connected and stand-alone PV applications (Gonzalez Montoya et al., 2016).

To obtain a system model, the PV module is represented by a Norton equivalent as it is shown in Figure 1: the current source I_{SC} and resistor R_{MPP} represents the short circuit current and instantaneous impedance of the PV module at the operating point, respectively. L is the inductor, R_L represents the inductor losses, R_B is the battery resistance, R_{on} is the on-resistance of the MOSFET (Q_1), V_f is the diode (D_1) forward voltage and V_B is the battery open-circuit voltage. C_i and C_o are the input and output capacitor of the converter, while R_{ci} and R_{co} are the equivalent series resistance (ESR) of each capacitor (Petrone et al., 2007).

Figure 1. Circuit model for the PV system.


To determinate the modelling equations, it is necessary to analyze the circuit when Q_1 is ON and D_1 is OFF (N Femia et al., 2010). The resulting equations, shown below in (1) and (2), represent the current in C_i and C_o , respectively, while the inductor voltage is presented in (3). In those expressions I is the inductor current, V_{C_i} is the Voltage in Capacitor C_i and V_{C_o} is the Voltage in capacitor C_o . Moreover, the voltage on the PV module V_{pv} is reported in (4).

$$I_{C_i} = \lambda \cdot I_{SC} - \frac{V_{C_i}}{R_{MPP} + R_{C_i}} \lambda I \quad (1)$$

$$I_{C_o} = \frac{V_B}{R_B + R_{C_o}} - \frac{V_{C_o}}{R_B + R_{C_o}} \quad (2)$$

$$V_L = \lambda \cdot V_{C_i} + \beta \cdot I_{SC} - (R_L + R_{on} + \beta) \cdot I \quad (3)$$

$$V_{pv} = \lambda \cdot V_{C_i} + \beta \cdot I_{SC} - \beta I \quad (4)$$

Where:

$$\lambda = \frac{R_{MPP}}{R_{MPP} + R_{C_i}}, \beta = \frac{R_{C_i} \cdot R_{MPP}}{R_{MPP} + R_{C_i}} \quad (5)$$

In the previous equations the factor λ corresponds the percentage of current flowing by C_i capacitor due to the resistive divisor formed by R_{MPP} and R_{C_i} , while β corresponds to the equivalent parallel resistance formed by both R_{MPP} and R_{C_i} .

The other state of the circuit is obtained when Q_1 is OFF and D_1 is ON. In this case, the equations describing the current on C_i and the PV voltage V_{pv} are the same as in the previous case, therefore equations (1) and (4) hold. The resulting equations for the current in C_o and the inductor voltage V_L are shown in (6) and (7), respectively.

$$I_{Co} = \theta \cdot I + \frac{V_B}{R_B + R_{Co}} - \frac{V_{Co}}{R_B + R_{Co}} \quad (6)$$

$$V_L = \lambda \cdot V_{Ci} + \beta \cdot I_{SC} - (R_L + \gamma + \beta) \cdot I - V_f - \theta \cdot V_{Co} - \sigma \cdot V_B \quad (7)$$

In both (6) and (7), the factor γ corresponds to the equivalent parallel resistance formed by both R_B and R_{Co} , while the factors θ and σ correspond to the resistive divisor formed by R_B and R_{Co} . Those factors are reported in (8).

$$\gamma = \frac{R_B \cdot R_{Co}}{R_B + R_{Co}}, \theta = \frac{R_B}{R_B + R_{Co}}, \sigma = \frac{R_{Co}}{R_B + R_{Co}} \quad (8)$$

To obtain the set of equations representing the nonlinear system in any state, it is necessary to perform the volts-second balance at the inductor and the charge balance at each capacitor. From the volts-second balance, the resulting equation is shown in (9); from the charge balance at C_i and C_o , the obtained equations are shown in (10) and (11). Those three equations represent the nonlinear model of the PV system.

$$L \frac{dI}{dt} = \lambda \cdot V_{Ci} + \beta \cdot I_{SC} - (R_L + d \cdot R_{on} + \beta + (1-d) \cdot \gamma) \cdot I - (1-d) \cdot V_f - (1-d) \cdot \theta \cdot V_{Co} - (1-d) \cdot \sigma \cdot V_B \quad (9)$$

$$C_i \frac{dV_{Ci}}{dt} = \lambda \cdot I_{SC} - \frac{V_{Ci}}{\alpha} - \lambda I \quad (10)$$

$$C_o \frac{dV_{Co}}{dt} = (1-d) \cdot \theta \cdot I - \frac{V_{Co}}{\delta} + \frac{V_B}{\delta} \quad (11)$$

where factor α represents the equivalent series resistance of R_{MPP} and R_{Cp} , while δ represents the equivalent series resistance of R_B and R_{Co} :

$$\alpha = R_{MPP} + R_{Cp} \quad \delta = R_{Co} + R_B \quad (12)$$

To apply a linear control technique, the previous model must be linearized using the Jacobian technique as it is described in (Ahmed et al., 2011; Trejos et al., 2012). For this purpose, the selected state variables are V_{Ci} , I and V_{Co} ; the input variables are I_{SC} , V_B and d ; while the variable to be controlled is the PV voltage V_{pv} . The equations and matrices A, B, C and E used to perform a state space representation of the PV system are given in (13)-(14) and (15)-(18), respectively.

$$\dot{X} = AX + BU \quad (13)$$

$$Y = CX + EU \quad (14)$$

$$X = \begin{bmatrix} V_{Ci} \\ I \\ V_{Co} \end{bmatrix} U = \begin{bmatrix} I_{SC} \\ V_B \\ d \end{bmatrix} Y = [V_{pv}] \quad (15)$$

$$A = \begin{bmatrix} -\frac{1}{C_i \alpha} & -\frac{\lambda}{C_i} & 0 \\ \frac{\lambda}{L} & -\frac{R_L + \beta + (1-D) \cdot \gamma + D \cdot R_{on}}{L} & -\frac{(1-D) \cdot \theta}{L} \\ 0 & \frac{(1-D) \cdot \theta}{C_o} & -\frac{1}{C_o \cdot \delta} \end{bmatrix} \quad (16)$$

$$B = \begin{bmatrix} -\frac{\lambda}{C_i} & 0 & 0 \\ \frac{\beta}{L} & -\frac{(1-D) \cdot \sigma}{L} & \frac{V_f - (R_{on} - \gamma) \cdot I + \sigma \cdot V_B + \theta \cdot V_{Co}}{L} \\ 0 & \frac{1}{C_o \cdot \delta} & \frac{I \cdot \theta}{C_o} \end{bmatrix} \quad (17)$$

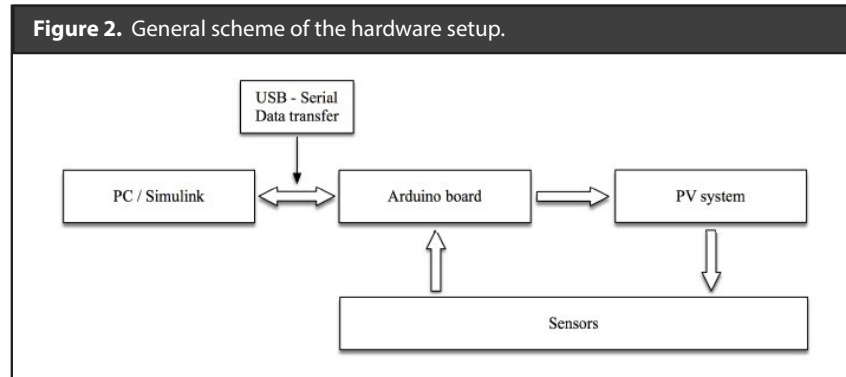
$$BC = [\lambda \quad -\beta \quad 0] \quad E = [\beta \quad 0 \quad 0] \quad (18)$$

PID controllers are usually designed to regulate the PV voltage, which is widely reported in both literature and industry (Ahmed et al., 2011; Trejos et al., 2012), hence this paper will include such a controller. However, the proposed methodology is also applicable to any control structure.

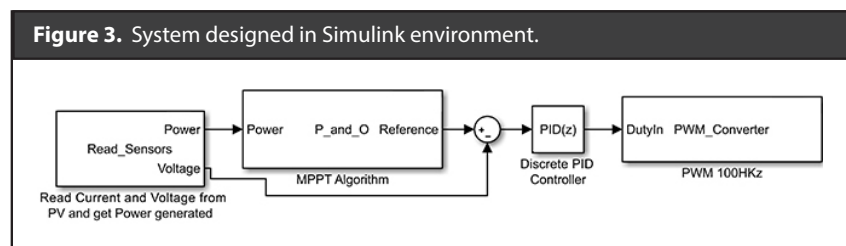
To design a PID controller, a transfer function ($G_{v_{pv}D}$) is obtained using the state-space model presented in (13)-(18), in which the duty cycle D is the control input and V_{pv} is the controlled variable.

Software and Hardware setup for RCP implementation

An overview of hardware setup is presented in Figure 2, where the "PV system" block represents the PV circuit described in Figure 1. In addition, an Arduino board is used as an interface between the PV system and the PC, which allows to acquire data from both voltage and current sensors to be transferred to Simulink. Moreover, the Arduino board receives control signals from Simulink, which are transferred to the PV system using an on-board PWM. This procedure is simple since the Matlab support package for Arduino enables to transfer Simulink block diagrams to Arduino boards using automatic code generation, offering an automatic serial communication protocol for information exchange. Finally the proposed platform controls the PV system using a Real Time Operation System (RTOS), which enables to update variables on real time (MathWorks, n.d.)



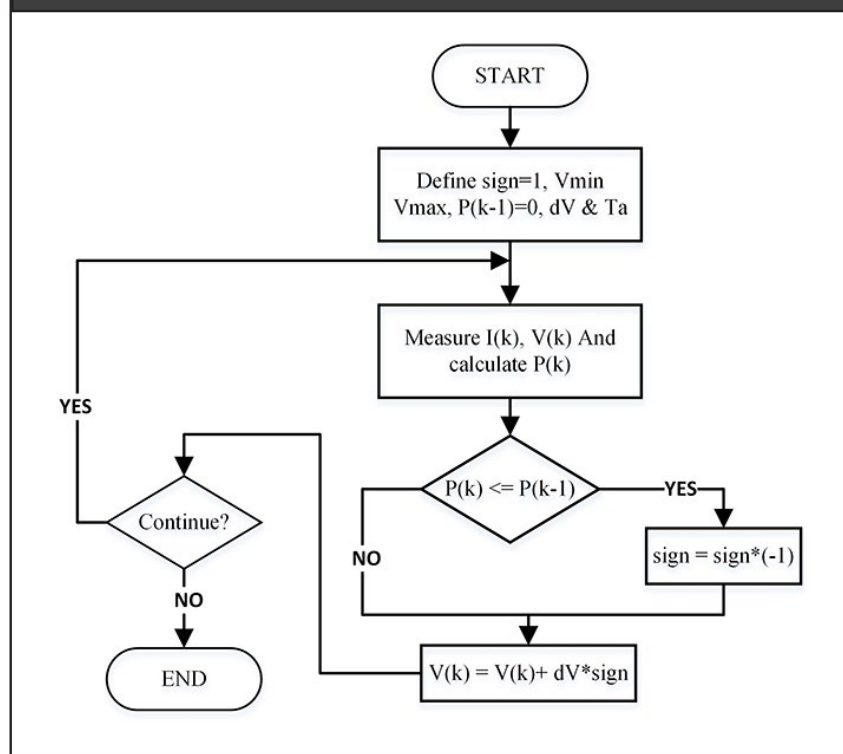
This work was performed using an Arduino Mega 2560 board. Such a board has 54 digital pins, 16 analogs to digital (ADC) inputs, 256 kB flash memory, and it can be programmed directly from the Simulink environment using the support package for Arduino hardware available in Mathworks website (Ibrahim et al., 2020). Simulink block diagrams were selected to reduce the programming knowledge required to operate the RCP PV system; however, the Simulink support package for Arduino enables to create personalized Simulink blocks for Arduino using the s-function builder. Finally, The Simulink implementation is shown in Figure 3.



In such a Simulink block-diagram, the *MPPT* block acquires the PV power through the sensors module, using such information to execute the traditionally Perturb and Observe (P&O) MPPT algorithm (N Femia et al., 2010; Nicola Femia et al., 2005). The flowchart of the P&O algorithm is presented in Figure 4, in which the variable *Sign* determines the direction of the perturbation, which is performed with a voltage amplitude dV and each perturbation period T_p . In this algorithm, the instantaneous PV power is compared with the previously measured PV power to determine the next perturbation direction; hence, the sign variable changes when the PV power has been decreased due to the previous perturbation. Such a procedure enables to find the PV voltage that guarantees the maximum power extraction, a detailed description of the P&O algorithm is given in (N Femia et al., 2010; Nicola Femia et al., 2005).

Consequently, the P&O algorithm sets the voltage that must be imposed to the PV system. Therefore, the P&O output is a voltage reference, which must be compared with the PV voltage to generate an error signal. Such an error is then processed by a discrete controller (*PID* block), as it is presented in Figure 3, to produce the required duty cycle of the DC/DC converter to ensure the desired PV voltage.

Figure 4. Perturb and Observe flowchart.



The Arduino code developed to acquire the voltage and current data from the sensors is reported in Box 1 of Figure 5, which scales the measured 10 bits values to a range of 5 V. Similarly, Box 2 of Figure 6 reports the code used to implement the P&O MPPT algorithm.

Figure 5. Arduino code to read voltage and current from sensors.

```

Box 1
void read_adc () {
    SF=5/1023;
    V = analogRead (0)*SF;
    I = analogRead (1)*SF;
    Power [0] = V*I;
    Voltage [0] = V;
}
    
```


Figure 6. Arduino code for the P&O MPPT algorithm.

```
Box 2  
if (P_act <= P_old)  
{  
    sign = sign*(-1);  
}  
V = V + dV*sign;  
if (V < Vmin)  
{  
    V = Vmin;  
}  
if (V > Vmax)  
{  
    V = Vmax;  
}  
P_old = P_act;
```

A PWM block is used to generate the activation signal of the MOSFET into the DC/DC converter, hence imposing the desired duty cycle. The presented $PWM_{converter}$ block (Figure 3) sets the PWM duty cycle and defines the switching frequency, 100 kHz in this case. The Arduino code to generate the PWM signal is based on (Müller et al., 2015) and presented in Box 3 of Figure 7: in that code the timer one is configured in fast PWM mode, with a pre-scaler equal to one, and in non-inverted mode. The $freq$ value is assigned to the $ICR1$ register to define the signal frequency, while the duty cycle value ($d1_1$) is assigned to the $OCR1A$ register. To ensure that the duty cycle is constrained to realistic values, the code given in Box 4 of Figure 7 was introduced into the $PWM_{converter\ block}$ in which $Dmin$ and $Dmax$ correspond to the minimum and maximum limits, respectively.

Figure 7. Arduino code to configure 100 KHz PWM.

```
Box 3  
freq=(F_ard/(P*F_pwm))-1;  
//P=prescaler=1  
pinMode(11, OUTPUT);  
TCCR1A = 0;  
TCCR1B = 0;  
// Duty channel A  
d1_1=freq*D1_1;  
//Set TOP value  
//for Timer 1.  
ICR1 = freq;  
OCR1A = d1_1;  
//Set ch A to  
//non-invert mode  
TCCR1A |= (1 << COM1A1);  
TCCR1A |= (0 << COM1A0);  
//Set chl B to  
//non-invert mode  
TCCR1A |= (1 << COM1B1);  
TCCR1A |= (0 << COM1B0);  
//En Fast PWM  
//with ICR1 as TOP  
TCCR1A |= (1 << WGM11);  
TCCR1B |= (1 << WGM12);  
TCCR1B |= (1 << WGM13);  
//Str timer  
//with prescaler 1  
TCCR1B |= (1 << CS10);  
TCCR1B |= (0 << CS11);
```

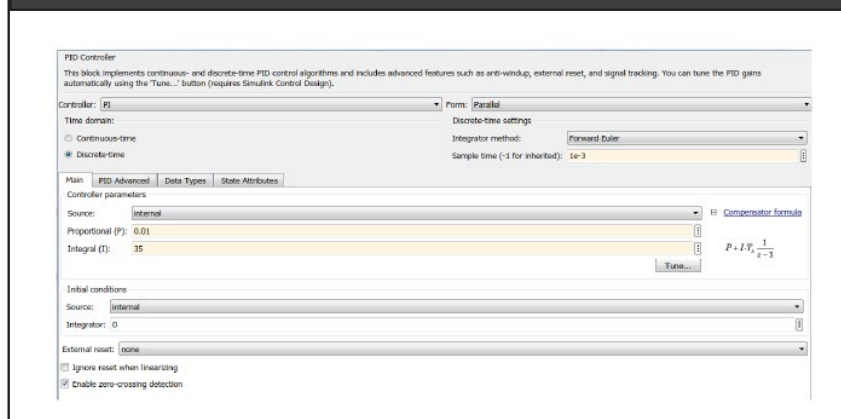
Figure 8. Arduino code to constrain duty cycle.**Box 4 Arduino code to constrain duty cycle**

```

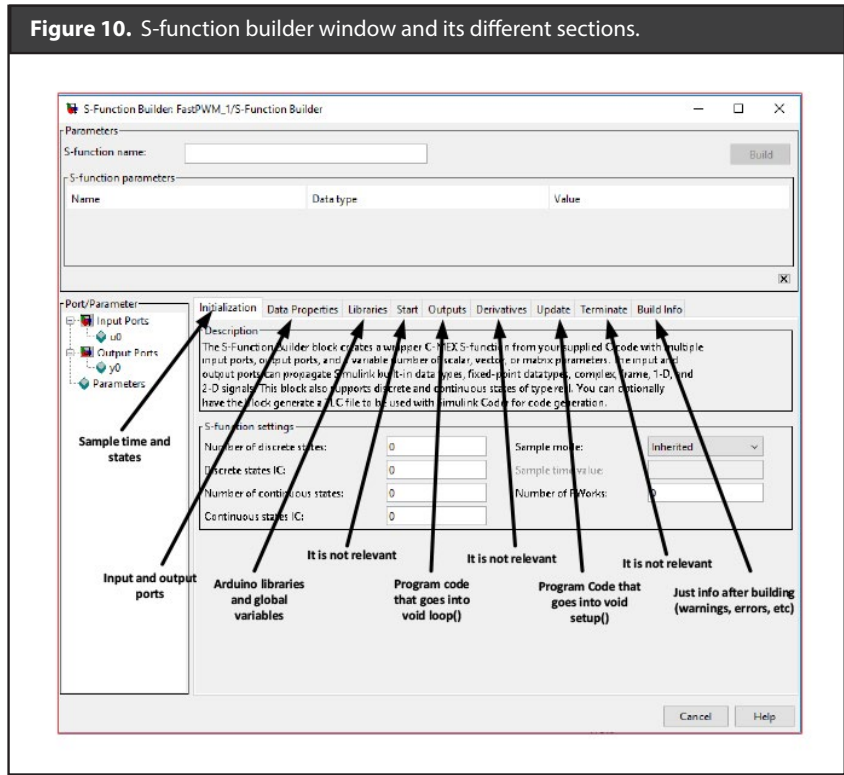
//Get D value from
//Controller block
D = dutyIn[0];
// constrain duty
//to Dmax
if (D > Dmax){
    D = Dmax;
}
//constrain duty
//to Dmin
if (D < Dmin){
    D = Dmin;
}
d=frec*D;
//set TOP value
//for timer 1
ICR1 = frec ;
OCR1A = d;

```

A discrete PID controller was used to perform the control loop for the PV voltage. This implementation was developed using the default Simulink block, which configuration dialog is presented in Figure 9; such a block makes possible to modify the transfer function form and the integration method. Moreover, the discrete PID controller requires to define a sample time based on the discretization process of the PV system model; for the Arduino Mega, the shortest sample time is one millisecond (1 ms). Finally, the forward Euler method was selected since a fixed step-size is needed for the RTOS.

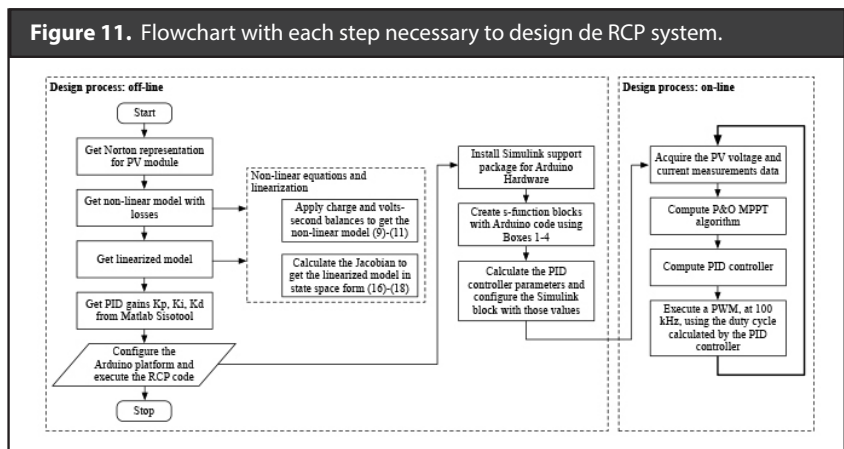
Figure 9. Configuration values for the PID controller block.

Finally, the Simulink block-diagram must be translated into Arduino code, which is done using the s-function builder. That builder is divided in different tabs, as it is shown in Figure 10: *Initialization tab* defines the Arduino's sampling time, and the input and output ports needed for the task are defined in the *Data properties* tab. Arduino libraries and global variables are included in the *Libraries* section. The *Outputs* tab is where the Arduino loop function is executed, while their configuration registers are initialized in the *Discrete update* tab. *Continues Derivatives* tab is not relevant for Arduino applications. Finally, Warnings and errors occurred after compiling are presented in the *Build info* section.



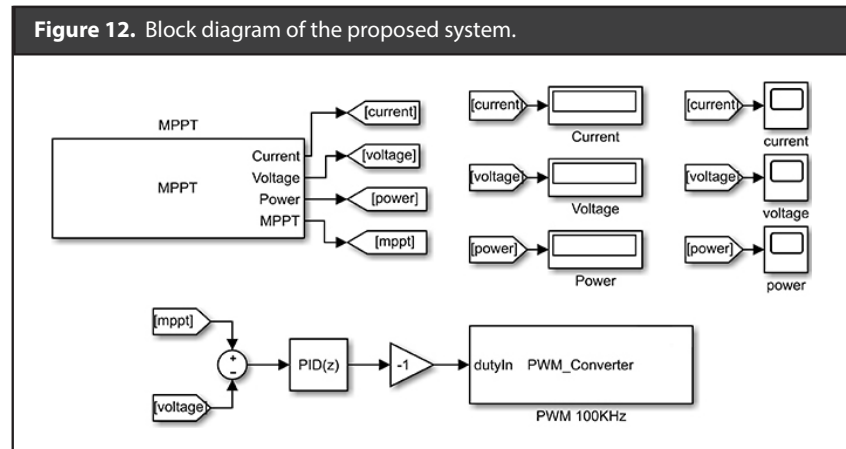
Summary of the RCP implementation

The flowchart for designing the RCP system is summarized in Figure 11: the first part, developed offline, consists in modeling the PV system, including parasitic losses. Then, such a model is linearized to enable the use of classical (but also newer) control techniques. Finally, the PV voltage controller is designed using the linearized model. The second part, the Arduino platform is configured by means of the Simulink/Matlab support software for Arduino, which also produces the Arduino code for the RCP process. Finally, the third part of the procedure corresponds to execute, on-line, the Arduino code on the RCP platform, which enables to test the PV system under realistic conditions.

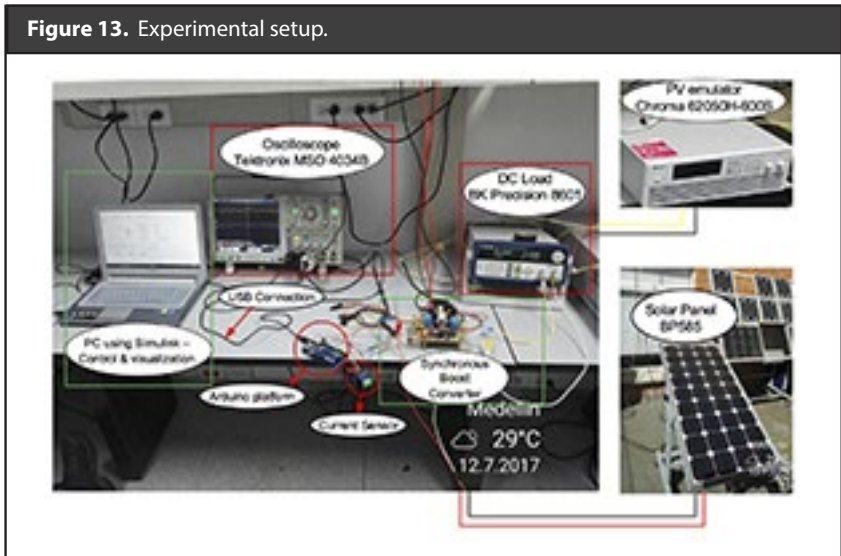


Results and Discussion

The proposed platform to extract the maximum energy from a PV module using both a P&O MPPT algorithm and a PID controller is presented in the Simulink block-diagram given in Figure 12. The Arduino board acquires the PV voltage (V_{PV}) and current (I_{PV}) measurements, send such data to Simulink, and receives the control action to generate the PWM signal. This platform enables the visualization of variables such as V_{PV} , I_{PV} , and PV power (P_{PV}), which are available into the Simulink environment. Finally, an USB connection was used to communicate both Arduino and Simulink (into a PC).



The experimental setup developed to validate the proposed RCP system is presented in Figure 13. A Chroma 62050h-600s PV emulator was used to perform experiments under controlled (and reproducible) ambient conditions. A BP585 PV module and a PV current sensor (ACS712) were included for validation purposes. A boost converter was developed to interface the PV source with a commercial DC load (BK precision 8601), which was set to 24 V, but voltage changes were forced during the experiments to test the RCP system. A Tektronix MSO 4034B oscilloscope was used to register measurements from the PV voltage and current, load voltage, and to calculate PV power; those data are used to validate the RCP performance. The RCP system was designed using an Arduino Mega 2560 (Italy version), and a PC with Simulink was used to program the Arduino Mega and for both visualization and interaction with the Arduino board. Finally, the parameters of the PV module, DC-DC converter, and DC bus are presented in Table 1.



The Chroma software enables the configuration of the Chroma 62050h-600s to emulate a PV module using the following parameters: P_{mpp} , V_{mpp} , and temperature. As it is presented in Figure 14, the software generates the current vs voltage ($I - V$) and power vs voltage ($P - V$) curves and shows the instantaneous operating point of the emulated PV module. The figure shows the $P - V$ curves for both $750\text{W}/\text{m}^2$ (green line) and $500\text{W}/\text{m}^2$ (gray line). The emulated irradiance is configured using buttons that change the percent of irradiance, at standard test conditions (STC), reaching the PV module. Finally, the software shows the PV module parameters corresponding to the irradiance and temperature values.

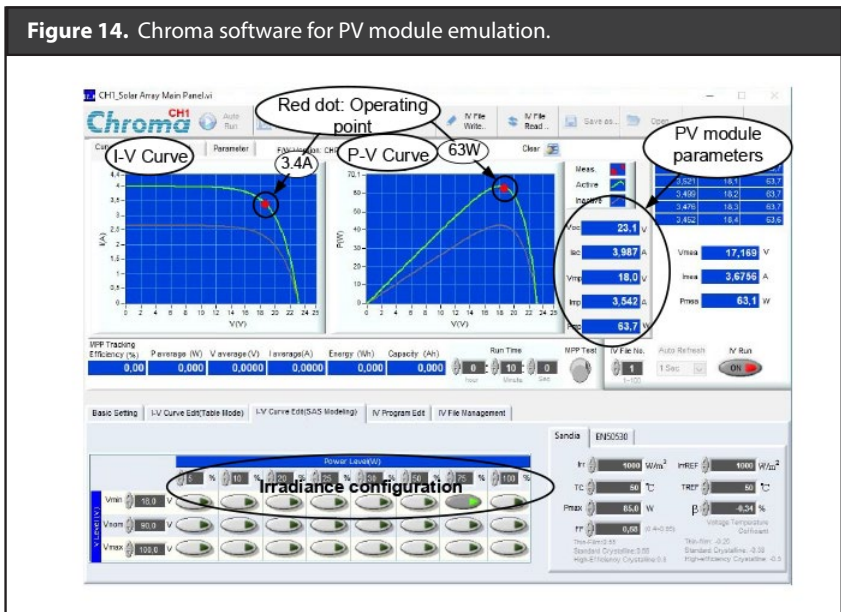


Table 1. System parameters.

Solar Panel Parameters at STC		
Maximum power	P_{mpp}	85 W
Voltage at Pmax	V_{mpp}	18 V
Current at Pmax	I_{mpp}	4.72 A
Short-circuit current	I_{SC}	5 A
Open-circuit voltage	V_{OC}	22.1 A
Temperature coefficient of I_{SC}	α_I	0.065%/°C
Temperature coefficient of voltage	α_V	-80mV/°C
Converter parameter		
Input capacitor	C_i	22 μ F
Output capacitor	C_o	22 μ F
Inductor	L	330 μ H
Inductor resistance	R_L	60m Ω
ON resistance Mosfet	R_{ON1} and R_{ON2}	35m Ω
DC Load parameters		
DC load equivalent resistance	R_B	60m Ω
DC load voltage	V_B	24V

Simulation Results

Using the state space model presented in (16)-(18), the transfer function $G_{V_{pv}D}$ given in (19) was obtained. Then, using SISOTOOL from Matlab and the discretized transfer function, the parameters of a discrete PI controller were obtained using a sample time equal to 1 ms. The controller design, for this example, considers a settling time equal to 50 ms and a damping ratio equal to 0.707, obtaining the following parameters: $K_p D = 0.01$ and $K_i D = 35$. The parameters of the MPPT algorithm, which are the perturbation period $T_a = 740$ ms and size $dV = 1$ V, were calculated following the procedure reported in (Nicola Femia et al., 2005). To validate the designed PI controller, a circuital simulation was performed in the PSIM simulator, using an implementation of the circuit model presented in Figure 1. Both irradiance and DC load voltage perturbations were considered to test the MPPT algorithm effectiveness and PI controller response.

$$G_{V_{pv}D} = \frac{-444.6s^2 - 3.64 * 10^9s - 2.059 * 10^{15}}{s^3 + 6.07 * 10^5s^2 + 7.73 * 10^8s + 8.361 * 10^{13}} \quad (19)$$

Figure 15 shows the system behavior under an irradiance change from 750W/m² to 500W/m². In such a simulation the PV voltage (blue line) shows a typical three-step oscillation around V_{MPP} which means that the P&O algorithm has reached the MPP (Nicola Femia et al., 2005). Moreover, despite the irradiance change, the V_{MPP} value is not perturbed due to the correct action of the PI controller. The simulation also

reports the PV current (magenta line) change, from 3.47A to 2.36A, when the irradiance is perturbed. The same behavior is observed in the Pv power (red line), which changes from 62W to 41W. In a similar way, Figure 16 shows the simulation of the PV system when the irradiance increases from $500W/m^2$ to $750W/m^2$, obtaining symmetrical results. In both cases the PI controller works as expected, and the PV voltage follows the MPPT reference with a settling time shorter than 50 ms.

Figure 15. Simulation of the PV system under an irradiance change from to $500 W/m^2$.

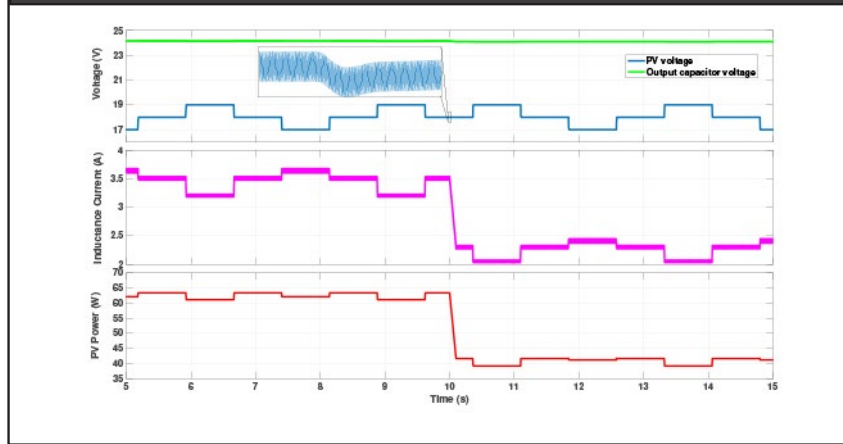


Figure 16. Simulation of the PV system under an irradiance change from $500 W/m^2$ to $750 W/m^2$.

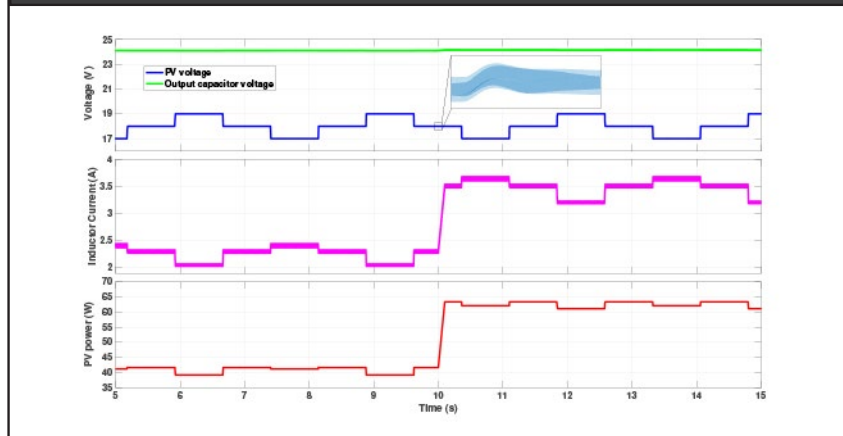
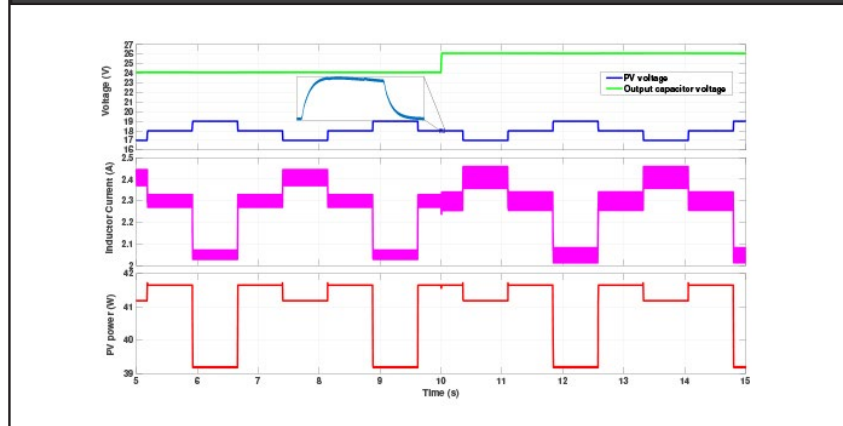


Figure 17 presents the simulation of the PV system, operating with an irradiance of $500W/m^2$, under a load voltage variation from 24 V to 26 V, which produces perturbation in both PV voltage and current. As in the previous cases, the PI controller mitigates those perturbations in less than 50 ms by changing the duty cycle. Hence, the operating point of the PV module remain at the MPP regardless the load voltage variation.

Figure 17. Simulation of the PV system under a load voltage change from 24 V to 26 V.



Experimental Results

Figure 18, Figure 19 and Figure 20 show experimental data collected using the PV emulator and the RCP platform. Data in Figure 18 was taken using an irradiance value of 750 W/m^2 . Such an experiment shows that the PV voltage reached the MPP, which is verified in the three-level behavior typical of steady-state P&O algorithms. Moreover, the experimental platform produces 63 W, which corresponds to the MPP power defined by the PV emulator as observed in Figure 14 (red dot). Finally, the settling time of the PV voltage in this experiment is near 50 ms, which is in agreement with the simulation results.

Figure 18. Load voltage, PV voltage, current and power at 750 W/m^2 .

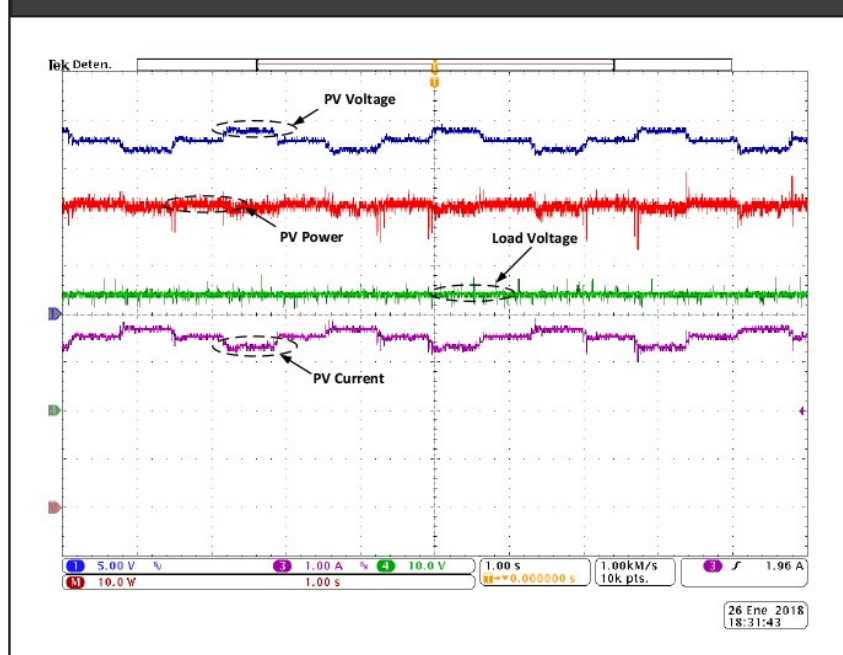


Figure 19 shows the system behavior due to irradiance changes. First, at a 500 W/m^2 irradiance value, the PV voltage fluctuate around 18 V and the PV current is around 2.3 A. Moreover, the PV power delivered is approximately 42W. When the irradiance reaches 750 W/m^2 , the PV voltage remains around 18 V due to the action of both the PI controller and the MPPT algorithm, which is a correct value according to the P-V curves presented in Figure 14. Instead, the PV current is increased to 3.3 A and the PV power reaches the MPP value of 63 W. In addition, during all the experiment, the three-step behavior on the PV voltage put into evidence the operation at the MPP of both irradiance conditions. Finally, this experiment shows the viability of the RCP platform for testing the controllers and MPPT algorithms designed for PV systems; which in this example, corresponds to a PI controller and a P&O algorithm, but any other controller and MPPT algorithm can be tested.

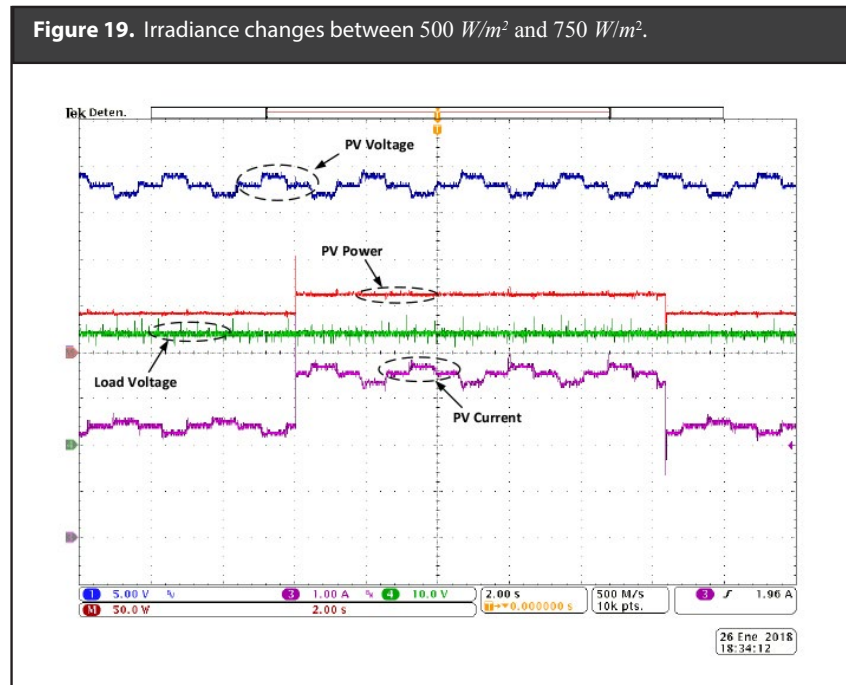
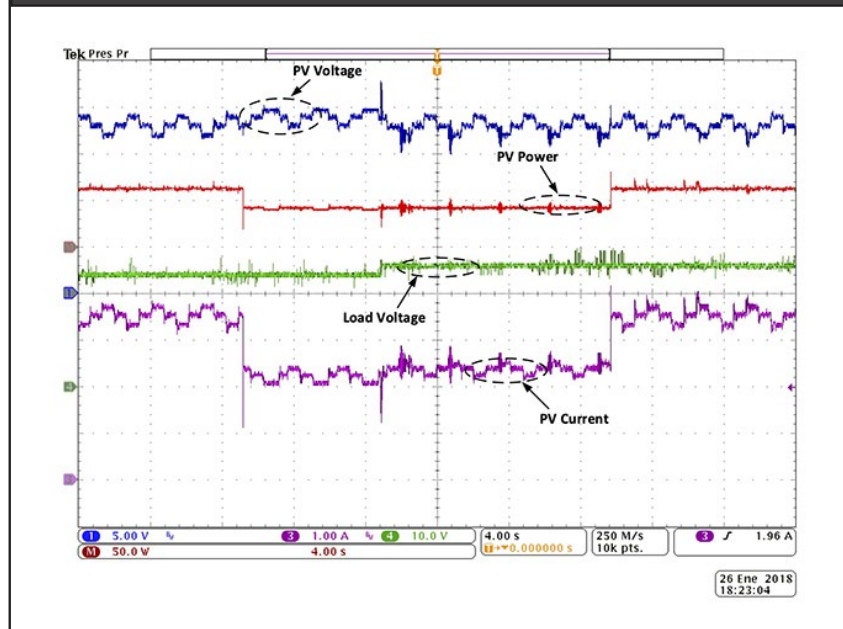


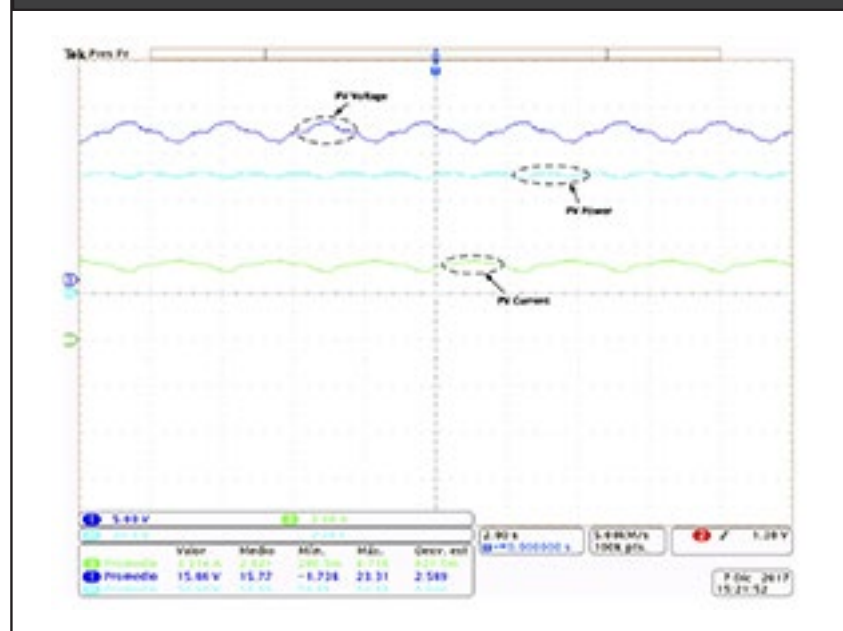
Figure 20 shows another experiment, in which both irradiance and load voltage are perturbed. As in the previous cases, the correct MPPT operation is verified by the three-step behavior in the PV voltage. Moreover, when the load voltage changes from 24 V to 26 V, the PV voltage successfully tracks the optimal V_{MPP} value in almost 6 seconds. Hence, despite both irradiance and load variations, the available maximum PV power is extracted.

Figure 20. Changes in both load voltage and irradiance.



Finally, data obtained with a real PV module (BP585) is presented in Figure 21. In this experiment the PV voltage is around a V_{MPP} equal to 16V, with a three-step behavior that ensures the operation at the MPP: I_{MPP} is 3.2 A and P_{MPP} is 51 W. Therefore, the RCP platform also works properly with real PV generators.

Figure 21. Data taken using a real PV module BP585.



Conclusions

The Arduino platform and Simulink environment have been used to develop a rapid control platform for PV applications. This platform enables the testing of different control strategies and MPPT algorithms in a simple way, hence reducing the prototyping time, which also decreases the final implementation cost. The RCP platform is capable of measuring, in real-time, relevant variables for diagnosis purposes of the PV module, DC/DC converter and control strategies.

A proof-of-concept prototype was developed to validate the proposed RCP platform. The results demonstrated the feasibility of the proposed platform to test both voltage controllers and MPPT algorithms in real conditions; those results were conducted with an industrial-level PV emulator and with a commercial PV panel.

Finally, the proposed RCP system can be used to test any controller based on PWM techniques, since such a modulation was considered in the design process. Therefore, controllers based on other modulators, such as variable-frequency sliding-mode controllers, cannot be tested in this RCP system. Such an application will be addressed in a future improvement by considering the control action over the switched model, but some problems must be faced: processing the PV model with variable switching frequency requires new integration methods and faster processing devices, which could be unobtainable in low-cost Arduino boards.

Acknowledgment

This work was supported by the José Domingo Pérez school of Engineering at the Universidad del Turabo and its CIESESE Consortium, an initiative funded by the U.S. Department of Energy (DE-NA0003330). This work was also supported by the Automatic, Electronic and Computer Science research group of the Instituto Tecnológico Metropolitano under the project P17211, the Universidad Nacional de Colombia and Colciencias (Fondo nacional de financiamiento para ciencia, la tecnología y la innovación Francisco José de Caldas) under the project "Estrategia de transformación del sector energético Colombiano en el horizonte de 2030 - Energetica 2030" - "Generación distribuida de energía eléctrica en Colombia a partir de energía solar y eólica" (Code: 58838, Hermes: 38945).

References

- Arellano-Monterrosas, J. L. (1994). Degradación del Suelo por Erosión Hídrica en Chiapas: Evaluación y Principios Tecnológicos para su Control, tesis (Ingeniero Agrónomo), México, Universidad Autónoma de Chapingo, pp. 149-251.
- Arellano-Monterrosas, J. L. (2005). Apropiación Territorial, Degradación Ambiental y Gestión de Recursos Hídricos en la Cuenca Superior del río Custepec, Chiapas, tesis (Maestría en Ciencias), México, Universidad Autónoma de Chapingo, pp. 46-481.
- Bauman, J. and Arellano-Monterrosas, J. L. (2003). Measuring Rainfall Erosivity Characteristics and Annual R-Factors for Adjustment of the USLE in a Tropical Climate. In: 25 years of assessment of erosion-proceedings. Ghent, Belgium. D. Gabriels and W. Cornelis (eds.), pp. 69-74.
- Campos-Aranda, D. F. (2010). Verificación de la Homogeneidad Regional Mediante Tres Pruebas Estadísticas. *Tecnología y Ciencias del Agua*, 1(4) octubre-diciembre, pp. 157-165. Disponible en: <http://www.revistatyca.org.mx/ojs/index.php/tyca/article/view/78>. [Consultado 25 de julio de 2019]
- Campos-Aranda, D. F. (2011). Estimación de Envolventes de Diseño por Subregiones

- Hidrológicas. *Tecnología y Ciencias del Agua*, 2(4) octubre-diciembre, pp. 175-194. Disponible en: http://www.scielo.org.mx/scielo.php?script=sci_arttext&pid=S2007-24222011000400012&lng=es&nrm=iso. [Consultado 25 de julio de 2019]
- Castro-Quintero, A. F., Lince-Salazar, L. A. y Riñao-Melo, O. (2017). Determinación del Riesgo a la Erosión Potencial Hídrica en la Zona Cafetera del Quindío, Colombia. *Revista de Investigación Agraria y Ambiental*, [e-journal] 8(1) enero-junio, pp. 17-26. Disponible en: <https://doi.org/10.22490/21456453.1828>. [Consultado 5 de julio 2019].
- Challenger, A. y Dirzo, R. (2009). Estado de Conservación y Tendencia de Cambio, Primera parte: Factores de cambio y estado de la biodiversidad, En: CONABIO: Capital Natural de México, Vol. 2, México, pp. 35-73.
- CORTOLIMA (2006). Fase de diagnóstico: Pérdida de Suelos. En: Plan de Ordenación y Manejo de la Cuenca Hidrográfica Mayor del Río Totare [e-book]. Ibagué, Colombia: Corporación Regional Autónoma de Tolima, pp. 834-838. Disponible en: http://www.cortolima.gov.co/sites/default/files/images/stories/centro_documentos/pom_totare/diagnostico/m_212perdida_de_suelos_totare.pdf. [Consultado 30 julio 2019].
- Cuevas, M. L., Garrido, A., Pérez-Damián, J. L. y Iura-González, D. (2010). Procesos de Cambio de Uso de Suelo y Degradación de la Vegetación Natural, En: INECC: Las Cuencas Hidrográficas de México, pp. 96-103.
- Desmet, P. y Govers, G. (1996). A GIS Procedure for Automatically Calculating the USLE LS Factor on Topographically Complex Landscape Units. *Journal of Soil and Water Conservation*, 51(5), pp. 427-433. Available at: <http://search.ebscohost.com/login.aspx?direct=true&db=edsagr&AN=edsagr.US9633753&lang=es&site=eds-live>. [Accessed 24 June 2019].
- Durigón, V. L., Antunes, M. H., Sánchez de Oliveira, P. T., Fonseca de Carvalho, D. and Fernandes, M. M. (2014). NDVI Time Series for Monitoring RUSLE Cover Management Factor in a Tropical Watershed. *International Journal of Remote Sensing*, [e-journal] 35(2), pp. 441-453. Available at: <https://doi.org/10.1080/01431161.2013.871081>. [Accessed 26 June 2019].
- ESRI (Environmental System Research Institute), 2017. ArcGis Desktop/ArcMap 10. [Computer Program]. Redlands, California, U.S.A.: Environmental System Research Institute Inc.
- Fabián-Rivera, J. G., Mejía-Zermeño, R., Soto-Cortéz, G. y Val-Segura, R. (2005). Aspectos de la Medición de Sedimentos. En: Rivera-Trejo, F., Gutiérrez-López, A., Val-Segura, R., Mejía-Zermeño, R., Sánchez-Ruiz, P. A., Aparicio-Mijares, J., y Díaz-Flores, L. L., eds. *La Medición de Sedimentos en México*. Jiutepec, Morelos: IMTA-UJAT, pp. 11-15.
- FAO. (2006). World Reference Base for Soil Resources 2006. A Framework for International Classification, Correlation and Communication, Roma, FAO, 2006.
- Flores-López, H. E., Martínez-Menes, M., Oropeza-López, J. L., Mejía-Saens, E. y Carrillo-González, R. (2003). Integración de la EUPS a un SIG para Estimar la Erosión Hídrica del Suelo en Una Cuenca Hidrográfica de Tepatitlán, Jalisco, México. *Terra Latinoamericana*, 21(2) abril-junio, pp. 233-244. Disponible en: <https://www.redalyc.org/articulo.oa?id=573/57315595010>. [Consultado 13 de junio 2019].
- Gottschalk, C. L. (1964). Sedimentation. Part. I. Reservoir Sedimentation, In: Chow, V. T. *Handbook of Applied Hydrology: A Compendium of Water-Resources Technology*, Section 17-I, New York: McGraw-Hill, pp. 1418.
- Hexagón Geospatial, 2017. Erdas Imagine 8.3. [Computer Program] Stockholm, Sweden: Hexagon AB Inc.
- Krysanova, V., Williems, J., Bürger, G. and Österle, H. (2002). The Linkage Between Hydrological Processes and Sediment Transport at The River Basin Scale: A Modelling Study, In: Summer, W. y Walling, D. E., eds. *Modelling Erosion, Sediment Transport and Sediment Yield*, Thechnical Documents in Hydrology. No. 60. Paris, France: UNESCO-IHP, pp. 147-174.
- Pereyra-Díaz, D., Gómez-Romero, L. y Loeza-Hernández, F. (2005). Pérdida de Suelo por Erosión Hídrica, En: Rivera-Trejo, F., Gutiérrez-López, A., Val-Segura, R., Mejía-Zermeño, R., Sánchez-Ruiz, P. A., Aparicio-Mijares, J., y Díaz-Flores, L. L., eds. *La Medición de Sedimentos en México*. Jiutepec, Morelos: IMTA-UJAT, pp. 61-84.

- Pérez-Nieto, S. (2013). Erosión Hídrica en Cuencas Costeras de Chiapas y Estrategias para su Restauración Hidrológico Ambiental, tesis (Doctorado en Ingeniería), México, Colegio de Posgraduados, pp. 2.53-2.67.
- Secretaría de Recursos Hidráulicos. (1972). Segunda Parte: Datos Hidrométricos y de Aca-
rreo de Azolves en Suspensión, En: Boletín Hidrológico Núm. 38: Regiones Hidrológicas
Núm. 30 (Grijalva Usumacinta), Núm. 31 (Yucatán oeste), Núm. 32 (Yucatán norte) y
Núm. 33 (Yucatán este), Tomo I. México, D. F.
- USGS (United States Geological Survey). (2018). GloVis. (United States Department of the
Interior). [Online] Retrieved from <https://glovis.usgs.gov/app>.
- Walling, D. E. (2009). The Impact of Global Change on Erosion and Sediment Transport by
Rivers: Current Progress and Future Challenges. The United Nations World Water As-
sessment Program. Scientific Paper. Paris, France: UNESCO-IHP, pp. 2-22.
- Wischmeier, W. H. y, Smith, D. D. (1978). Agriculture Handbook 537: Predicting Rainfall
Erosion Losses, a Guide to Conservation Planning, Washington DC, USA: United States
Department of Agriculture, pp. 4-34.